

Chapter 30

Nanofluidics Fabricated by 3D Femtosecond Laser Processing



Koji Sugioka

Abstract Nanofluidics involves miniaturized fluidic devices containing a structure in which at least one dimension is in the nanoscale. Applications of nanofluidics include not only sensing and diagnosis of single molecules and separation of nanoscale objects such as deoxyribonucleic acid (DNA) but also the study of cancer cell migration. For the fabrication of nanofluidics, photolithography-based semiconductor processing and soft lithography are common techniques. Alternatively, femtosecond laser processing is a promising tool due to its distinct features, such as high fabrication resolution, high flexibility, high versatility, and three-dimensional (3D) fabrication capability. In particular, 3D fabrication capability, which enables both top-down (subtractive) and bottom-up (additive) schemes for nanofluidic fabrication, offers a great advantage over other techniques. The top-down scheme involves liquid-assisted femtosecond laser drilling and femtosecond laser-assisted etching (or femtosecond laser irradiation followed by chemical etching). Minimum width of nanochannel fabricated by this scheme is several hundred nanometers. To achieve the width narrower than 50 nm, a new strategy is proposed. The bottom-up scheme is represented by two-photon polymerization, which can create almost arbitrary 3D micro- and nanostructures with a high fabrication resolution of 100 nm or even smaller. This chapter is a comprehensive review of nanofluidics fabricated by 3D processing using femtosecond lasers, focusing on the features and methodologies of femtosecond lasers for nanofluidic fabrication, challenges for downsizing the nanochannel dimensions, and some applications of fabricated nanofluidics with future prospects.

Keywords Nanofluidics · 3D fabrication · Nanofabrication · Additive processing · Subtractive processing · Hybrid femtosecond laser processing · Biological application

K. Sugioka (✉)
RIKEN Center for Advanced Photonics, Wako, Saitama, Japan
e-mail: ksugioka@riken.jp

1 Introduction

Microfluidics is the technology to manipulate a small volume of fluid (on the order of femtoliters to microliters) and typically involves fluidic channels with dimensions of tens to hundreds of micrometers [1]. It can miniaturize a laboratory, reducing systematic labor, expenses, and sample consumption. Thus, microfluidics has revolutionized a variety of fields including chemistry, biology, medicine, physics, and engineering with applications such as microreactors, micro total analysis systems, lab-on-a-chip (LOC) devices, deoxyribonucleic acid (DNA) chips, inkjet printers, and micro-propulsion. Rapid advancement of this technology prompted us to further downsize the dimensions of systems to the nanoscale for challenging the physics of fluid flow in ultrasmall channels and the possibility of single-molecule analysis. Thus, the new field of nanofluidics has emerged and is increasingly attracting attention due to applications of microarrays for DNA sequencing, microfluidic devices for polymerase chain reactions (PCRs), LOC devices for the synthesis and analysis of peptide and oligonucleotide libraries, and microchips for drug screening or for single-cell analysis. Nanofluidics is defined as the study and application of miniaturized microfluidic systems containing a structure in which at least one dimension is in the nanoscale, typically smaller than several hundred nanometers [2]. A typical nanofluidic system consists of nanochannels, nanopipettes, or nanopores. In Fig. 30.1, the length scales and techniques used to fabricate micro- and nanosystems are schematically summarized with applications [3].

Photolithography-based semiconductor processing [4] is among the most common techniques for the fabrication of nanofluidic systems. To create fine structures that are 10 nm in size or smaller, lithography using high-energy beams such as electrons [5] and ions [6] is employed. Soft lithography is an alternative technique that has the advantages of low cost, easy setup, and high throughput while also

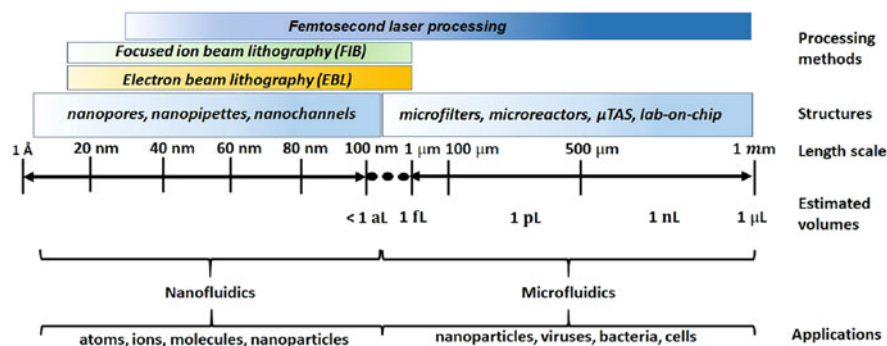


Fig. 30.1 Description of the length scales and common processing methods with applications used in micro- and nanosystems

enabling resolutions down to tens of nanometers, needed for nanofluidic domains [7]. It involves imprinting, molding, and embossing to replicate various structures on the substrates by using elastomeric stamps or molds. However, soft lithography necessitates the use of the other lithography methods mentioned above to create the stamp or mold masters.

Femtosecond lasers have become a promising technology for the fabrication of microfluidic systems owing to their distinct features such as high fabrication resolution, high flexibility, high versatility, and three-dimensional (3D) fabrication capability [8–13]. Femtosecond laser processing can be then extended to fabrication of nanofluidics. Its fabrication resolution which is defined as a minimum feature size achievable is, however, inferior to semiconductor processing. In fact, the minimum width of nanochannels fabricated by the femtosecond laser is several hundred nanometers [14]. In order to create nanofluidic systems with nanochannels narrower than 50 nm, new strategies were proposed [15]. Meanwhile, femtosecond laser processing offers some advantages over the semiconductor processing for fabrication of nanofluidics. One of the biggest advantages is its capability of true 3D structures, while the semiconductor processing can only create pseudo-3D structures, in other words, 2.5D structures. Another advantage is that the femtosecond laser processing can be adapted to a wide range of processing in terms of size, from nano to micro to even millimeter scale. Nanofluidic system is typically combined with microfluidic structures, and thus such a system can be obtained only by the femtosecond laser processing. Furthermore, the femtosecond laser processing allows the use of both top-down (subtractive) and bottom-up (additive) schemes to directly create 3D micro- and nanostructures. The top-down scheme involves liquid-assisted femtosecond laser drilling [14, 16, 17] and femtosecond laser-assisted etching (FLAE) (or femtosecond laser irradiation followed by chemical etching (FLICE)) [18–21]. The bottom-up scheme is best exemplified by two-photon polymerization (2PP), which can create almost arbitrary 3D micro- and nanostructures with a high fabrication resolution [22–25]. Importantly, performing the different schemes in succession, which is termed hybrid femtosecond laser 3D processing, enables creating much more complex 3D structures with enhanced functionalities [26–31], which are not achievable by the other techniques.

This chapter is a comprehensive review of nanofluidics fabricated by 3D femtosecond laser processing that details the features and methodologies of femtosecond laser processing for nanofluidic fabrication, challenges for downsizing the dimensions of nanofluidic systems, applications of fabricated nanofluidics, and future prospects. Although nanofluidics contains nanopores, nanopipettes, and nanochannels, this chapter focuses on only nanochannels because femtosecond lasers have so far been limited to the fabrication of nanochannels.

2 Features of Femtosecond Laser Processing for Nanofluidic Fabrication

2.1 Fabrication Resolution Far Beyond Diffraction Limit

The ultrashort pulse widths of a femtosecond laser (several tens to several hundreds of femtoseconds) can suppress the diffusion of the laser-induced heat from the exposed region because the deposition of laser energy into a material is completed before thermal diffusion occurs [32–34]. This means that the processed region is confined within the laser-exposed region, resulting in a higher fabrication resolution. The laser beam can be focused to a spot with a diameter comparable to or narrower than the laser wavelength by using an objective lens with a numerical aperture (NA) larger than 1. For example, when using a laser wavelength of around 500 nm, a focused spot size of 400–500 nm can be obtained to perform nanofabrication.

Ideally, the spatial energy distribution of a femtosecond laser beam has a Gaussian-like profile. Meanwhile, there exist threshold intensities only above which the process takes place on the basis of energy absorption. Thus, the processed area can be confined to the central area of the focal spot. Specifically, by adjusting the laser intensity to match the threshold intensity I_{th} indicated by a blue dashed line in Fig. 30.2a, the processed area is significantly narrowed relative to the beam diameter of the focused laser beam, $2W_0$, which is called threshold effect. By decreasing the laser intensity so that it approaches the threshold intensity at the center of the laser beam as shown in Fig. 30.2b, the processed area can be further narrowed.

Another important feature of a femtosecond laser is its extremely high peak intensity associated with the ultrashort pulse width, which easily exceeds 10^{15} W/cm². Such a high peak intensity can induce nonlinear absorption by materials whose bandgaps are larger than the photon energy of the laser beam, called multiphoton absorption [35, 36]. Since the absorption cross-section of m -photon absorption is proportional to the m -th power of the laser peak intensity, the effective beam diameter $2W$ for m -photon absorption becomes

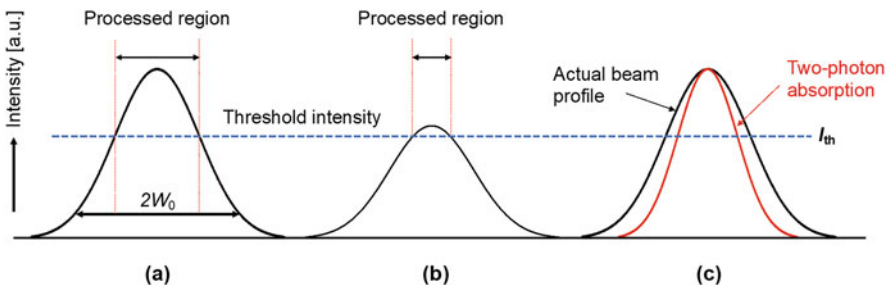


Fig. 30.2 The spatial intensity distributions of a focused Gaussian beam with (a) a higher intensity relative to the threshold for processing (dashed blue line) and (b) close to the threshold in a plane perpendicular to the beam axis. (c) Spatial intensity distributions absorbed by materials through single- (black) and two-photon (red) absorption of the focused Gaussian laser beam

$$2W = 2W_0/m^{1/2} \quad (30.1)$$

Consequently, the multiphoton absorption of a femtosecond laser by materials transparent to the laser beam can further improve the fabrication resolution as compared with single-photon absorption for the same wavelength, as shown in Fig. 30.2c, in which two-photon absorption has a narrower distribution than actual beam profile (single-photon absorption) [23, 37, 38]. Please note that single-photon absorption by half wavelength (second harmonics) provides higher resolution as compared with two-photon absorption by fundamental beam, because the beam diameter of second harmonics is a half that of the fundamental beam.

The synergetic contribution of the threshold effect and multiphoton absorption enabled the fabrication of nanohole arrays with sub-200-nm diameters in GaN substrates by ablation using a 387-nm-wavelength femtosecond laser [39]. The synergetic effect is also conducive to achieving typical fabrication resolutions of approx. 100 nm for 2PP even when using a near-infrared femtosecond laser [23]. These fabrication resolutions, which far exceed the diffraction limit of lasers, mean that femtosecond lasers are likely to find wider application in nanofluidic fabrication than conventional lasers.

2.2 3D Fabrication Capability

One of the most important features of femtosecond laser processing that makes it superior to other fabrication methods of micro- and nanofluidics is the capability of 3D processing, which relies on multiphoton absorption by transparent media including solids, liquids, and gases [38, 40, 41] (also see Chap. 10). As described above, the absorption cross-section of m -photon absorption is proportional to the m -th power of the laser peak intensity, which means the probability of multiphoton absorption depends on the laser peak intensity nonlinearly. Therefore, if the femtosecond laser beam is focused in the transparent medium at a moderate pulse energy, multiphoton absorption can be localized to be induced only at the focal volume where the highest laser intensity is generated in the laser beam path (Fig. 30.3a). As a result, the focal volume of the femtosecond laser inside the transparent medium is processed. 3D scanning of the focused femtosecond laser beam can then perform 3D processing of transparent media, such as glass and polymers, along the scanned trajectory of the focused laser beam (Fig. 30.3b).

The 3D fabrication capability of femtosecond lasers offers three types of schemes in 3D processing: undeformative, subtractive, and additive processing (see Fig. 30.4) [30]. The most common undeformative processing is permanent refractive index change, which is employed in 3D optical waveguide writing [42] and 3D data storage [43]. Subtractive processing can directly create 3D hollow structures at the micro- and nanoscale, typically in glass, by either liquid-assisted femtosecond laser drilling [14, 16, 17] or FLAE [18–21], which are utilized to

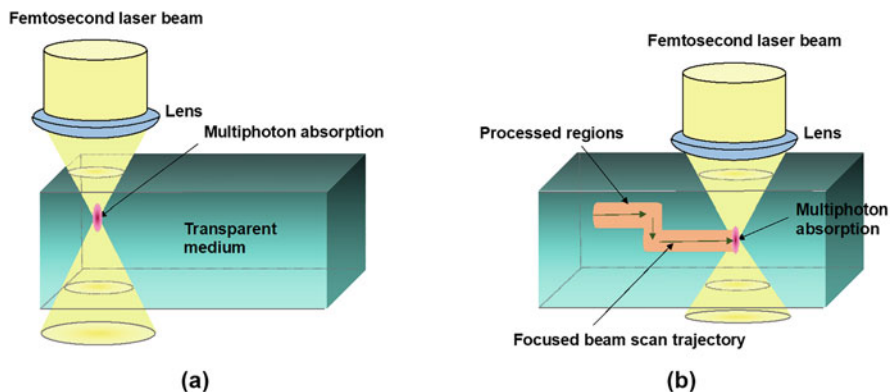


Fig. 30.3 Schematics of 3D fabrication of a transparent medium based on multiphoton absorption processes using a femtosecond laser. (a) When the femtosecond laser is focused at an adequate pulse energy inside the transparent medium, multiphoton absorption can be confined to the focal volume. (b) 3D scanning of focused femtosecond laser beam in the transparent medium performs 3D processing

fabricate micro- and nanofluidics. 3D polymer microstructure printing performed by TPP exemplifies additive processing and can create 3D micro- and nanostructures made of polymer with almost arbitrary shapes [22–25], which is also useful for nanofluidic fabrication. 2PP can be extended to 3D printing of other materials, such as metals [44, 45] and proteins [46, 47]. In the following section, more details of 3D glass micromachining techniques based on subtractive processing and additive 2PP of polymers are presented to highlight femtosecond laser-based technologies for nanofluidic fabrication.

3 Methods of Nanofluidic Fabrication by Femtosecond Laser

3.1 Top-Down (Subtractive) Method

In the subtractive processing, the laser-exposed regions are removed in a 3D manner. There are two main approaches to fabricating nanofluidic systems by subtractive femtosecond laser processing: liquid-assisted femtosecond laser drilling and FLAE. The former can be applied to a wide variety of materials as long as they are transparent to the laser beam. By contrast, only a limited number of materials can be processed by the latter approach. Femtosecond laser photolithography using positive-tone resists can also perform 3D subtractive processing for the fabrication of micro- and nanofluidic channels [48]. The following two subsections will detail liquid-assisted femtosecond laser drilling and FLAE.

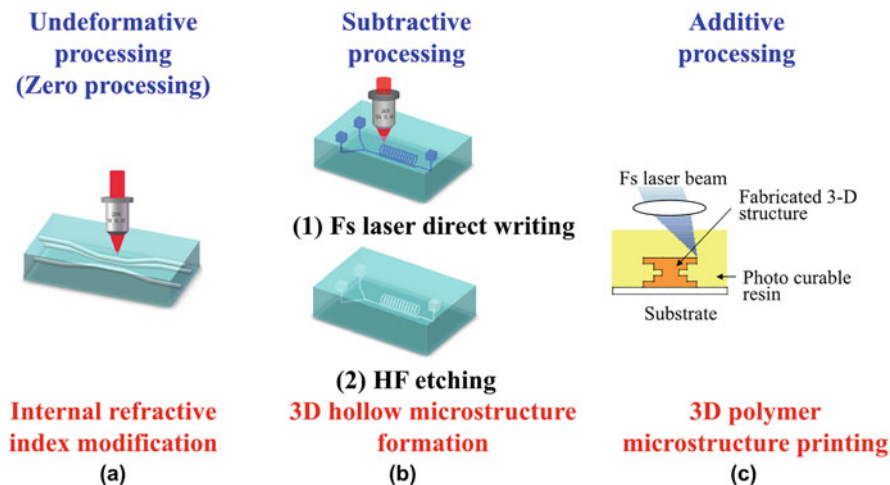


Fig. 30.4 Three different schemes in 3D processing achieved by femtosecond laser: (a) undeformative (e.g., internal refractive index modification), (b) subtractive (e.g., 3D hollow microstructure formation), and (c) additive (e.g., 3D polymer microstructure printing) [30]. (Reproduced with permission from the Institute of Physics. ©2019 by IOP)

3.1.1 Liquid-Assisted Femtosecond Laser Drilling

Liquid-assisted femtosecond laser drilling relies on the ablation of transparent materials in liquid, typically water, based on the multiphoton absorption of a femtosecond laser [14, 16, 17]. Specifically, the femtosecond laser beam is first focused on the side or rear surface of the transparent materials immersed in a liquid to initiate ablation and is then scanned toward the material's interior to create 3D drilled holes. This method can be applied to almost any material as long as it is transparent to the laser beam. In this method, the liquid serves the important role of efficiently removing the ablated material from the ablated site and avoiding the redeposition of debris, thus allowing the fabrication of long hollow channels of almost arbitrary shape. The fabrication resolution of this technique is determined by the spatial energy distribution of the focused femtosecond laser beam. The synergetic contribution of the threshold effect and multiphoton absorption enabled the fabrication of nanochannels longer than 200 μm with diameters of less than 700 nm [14].

To create nanochannels narrower than 100 nm, liquid-assisted femtosecond laser drilling of porous glass composed of approximately 95:5SiO₂-4B₂O₃-0:5Na₂O (wt%) was demonstrated using water. The porous glass contained a high density of pores with a mean size of 10 nm, distributed uniformly, forming a 3D connective network. Thus, water could be supplied efficiently to the ablation site through the pores, allowing the formation of long and narrow nanochannels. The ablated sample was finally annealed to form a glass compact by collapsing all the nanopores, while the micro- and nanochannels were trapped inside the glass [49]. Then,

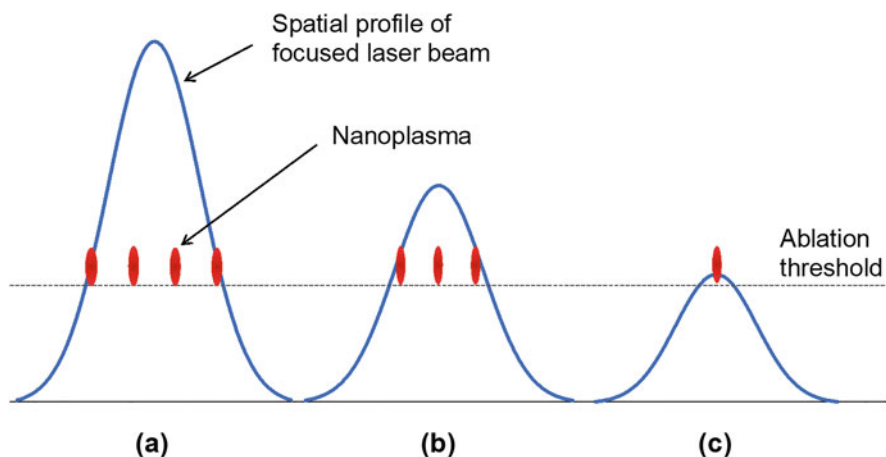


Fig. 30.5 Principle of single nanochannel creation based on nanoripple formation inside glass by femtosecond laser. (a) Nanoplasmas are generated at the focal spot due to spatial modulation of the energy deposition in the material with nanoscale periodicity. (b) As the laser intensity is reduced, the number of nanoplasmas decreases. (c) Further reducing the intensity very close to the ablation threshold at the center of the focused laser beam can generate only a single nanoplasma to create a single nanochannel by ablation [53]. (Reproduced with permission from De Gruyter. ©2016 by De Gruyter)

nanochannels were fabricated in the porous glass by using the phenomenon of nanoripple formation. It is well known that nanoripple structures are formed on the surface of, or inside, materials upon multiple pulse irradiation of a linearly polarized laser beam [50, 51] (also see Chap. 5). The periodicity of the formed ripple is much smaller than the laser wavelength (typically $1/10$ to $1/2$ of λ). Nanoplasma formation due to spatial modulation of the energy deposition in materials with nanoscale periodicity at the focal spot (see Fig. 30.5a) was proposed as a possible mechanism for nanoripple formation, although this is still under debate [52, 53]. Reducing the laser intensity decreases the number of nanoplasmas (Fig. 30.5b), owing to the threshold effect. Further reducing the intensity very close to the ablation threshold at the center of the focused laser beam can generate only a single nanoplasma (Fig. 30.5c), which ablates the glass to create a single-line nanochannel. Laser direct-write ablation of porous glass in water with well-controlled laser intensities has been employed to fabricate two-layered nanochannel arrays connected to two microchannels embedded $200\ \mu\text{m}$ below the glass substrate, as illustrated in Fig. 30.6a [15]. Figure 30.6b, c shows, respectively, an optical micrograph of the top view of two-layered nanochannel arrays and a cross-sectional scanning electron microscope (SEM) image of the nanochannels cut along the red dashed line in Fig. 30.6b. An SEM image of one of the nanochannels magnified from the white rectangle in Fig. 30.6c shows the formation of a nanochannel with a width of about $40\ \text{nm}$ and a height of about $1\ \mu\text{m}$ (aspect ratio of about 25) (Fig. 30.6d).

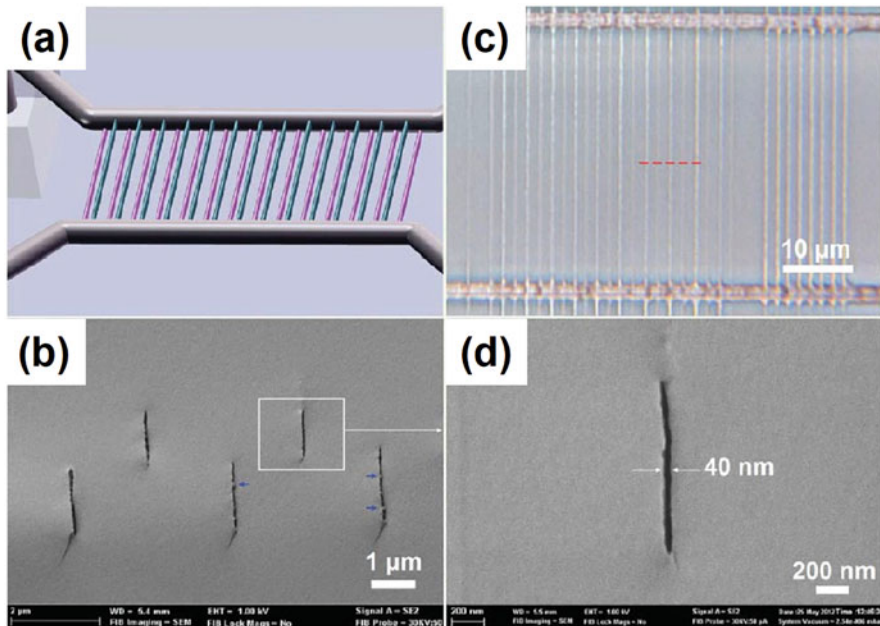


Fig. 30.6 Fabrication of nanochannels in porous glass by liquid-assisted femtosecond laser drilling. (a) Schematic of an array of double-layer nanochannels bridging two microchannels. (b) Top-view optical micrograph of double-layer nanochannels after post-annealing of drilled glass. (c) Cross-sectional SEM micrograph of the nanochannels cleaved along the red dashed line in (b). (d) Cross-sectional SEM micrograph of a nanochannel magnified from the white rectangle in (c) [15]. (Reproduced with permission from the Royal Society of Chemistry. ©2013 by RSC)

3.1.2 Femtosecond Laser-Assisted Etching

FLAE typically involves a two-step process, femtosecond laser 3D direct writing inside transparent materials followed by wet chemical etching, as illustrated in Fig. 30.3b [18–21]. During femtosecond laser direct writing, the chemical properties of the materials are modified as a result of multiphoton absorption, allowing the laser-exposed regions to be selectively etched away by wet chemical etching. The materials that can be processed by FLAE are limited to a few specific types of glass [18–21], sapphire [54], yttrium aluminum garnet crystals [55], and silicon [56]. Glass is used for nanofluidic applications, and there are two types of glass available for FLAE: photosensitive glass and fused silica. In the case of photosensitive glass, thermal treatment must be performed before etching to develop the modified regions in the laser-exposed region. For both types of glass, a diluted hydrofluoric (HF) acid solution (5–10%) is typically used as etchant for selective etching. Although the modification mechanisms of each glass type are completely different, the etching selectivity between the laser-exposed and unexposed regions is approx. 50 for both. The etching selectivity is the most important factor in determining the fabrication

resolution, so that the typical fabrication resolution by FLAE using HF is a few microns, which is inferior compared to liquid-assisted femtosecond laser drilling. Thus, it is challenging to fabricate nanofluidic channels by FLAE.

To create nanochannels in fused silica by FLAE, the strategy shown in Figs. 30.5 and 30.6 was employed. Line scanning of a single nanoplasma generated by the linearly polarized femtosecond laser beam created a modified line with a width of less than 100 nm and a length of 55 μm . Subsequent wet etching increased the channel width to 200 nm, which is still much less than 1 μm [57]. In the case of fused silica, selective etching can be performed using a potassium hydroxide (KOH) solution, which provides much higher etching selectivity than HF [58]. Therefore, KOH could improve the fabrication resolution, enabling the fabrication of nanofluidic channels narrower than 100 nm.

Post-thermal treatment is very effective for smoothing the etched surface of photosensitive glass to an average roughness better than 1 nm, which is crucial for some microfluidic applications [59]. Furthermore, the post-thermal treatment can transform the narrow microchannels in photosensitive glass formed by FLAE into nanochannels [60]. To fabricate nanofluidics in photosensitive glass, a microfluidic structure composed of two open microreservoirs connected to an embedded microreservoir with five narrow microchannels was designed. Figure 30.7a shows the optical micrograph of a sample after femtosecond laser direct writing followed by first thermal treatment, where the modified regions show up brown. The modified width of the narrow microchannels was approx. 2 μm . After wet etching in HF, the microchannels became tapered, owing to isotropic etching from both the left- and right-hand side open microreservoirs toward the center-embedded microreservoir (Fig. 30.7b). The narrowest width of the microchannels was measured to be approx. 4 μm at the junction of the center-embedded microreservoir, which was twice the modified width. The post-thermal treatment of the created microfluidic structure significantly deformed the microchannel structure, narrowing the width (Fig. 30.7c). To determine the dimensions of the deformed channels, the fabricated microfluidic structure was filled with a Rhodamine dye solution for fluorescence microscopy. Figure 30.7d, e shows a channel narrower than 1 μm and lower than 7 μm at the channel center. Channel width narrowing is likely responsible for the melting of the shallow glass surface layers during post-thermal treatment. Specifically, the temperature for the post-thermal treatment was set slightly below the glass melting point, which can melt the shallow surface layers of glass thanks to the lower surface energy, as compared to the bulk, needed to induce glass deformation and create architectures down to the nanoscale inside the microfluidic structures.

3.2 *Bottom-Up (Additive) Method*

Additive processing is used to construct solid 3D structures along the scanning trajectory of focused laser beam. The most common additive process using femtosecond lasers is 2PP, for which a photocurable epoxy resin or a negative-tone

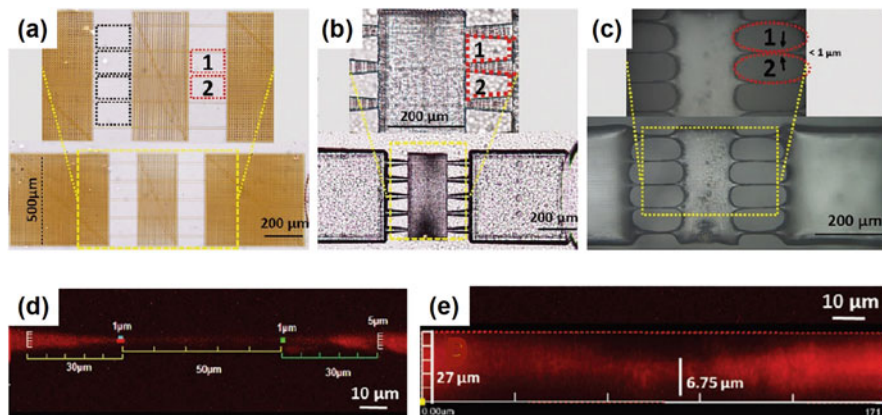


Fig. 30.7 Fabrication of nanofluidics in photosensitive glass by FLAE with post-thermal treatment. (a) Optical micrograph of sample after laser direct writing followed by first thermal treatment. Modified regions appear dark brown. (b) Optical micrograph of sample after chemical etching. (c) Optical micrograph of sample after post-thermal treatment. (d) Top and (e) cross-sectional fluorescence images of nanochannel filled with Rhodamine inside a microfluidic biochip [60]. (Reproduced with permission from Wiley. ©2020 by Wiley)

resist is utilized as precursor material [22–25] (also see Chap. 22). These precursors are transparent to the wavelength of a femtosecond laser (typically, visible or near-infrared) and solidify (polymerize) by two- (or multi-) photon absorption only at the focal volume. 3D scanning of the focused femtosecond laser in the precursor yields 3D micro- and nanostructures of almost arbitrary shape. Importantly, the fabrication resolution of 2PP is typically approx. 100 nm when using an objective lens with an NA larger than 1, which is much smaller than the diffraction limit of the laser beam, owing to the synergetic contributions of two-photon absorption and the threshold effect [23].

One drawback of 2PP is that it requires an extremely long time to create a volume structure such as a microfluidic chip owing to the nature of bottom-up fabrication using a tightly focused laser spot. Thus, 2PP is only used to integrate nanofluidic channels in microfluidic channels pre-fabricated by other methods. For the fabrication of nanofluidic systems, 2PP was combined with conventional UV photolithography [61]. First, SU-8 photoresist was spin-coated on a Si wafer. Then, UV light was directed through a film mask to create two separated microfluidic structures, followed by femtosecond laser direct writing to connect the two microfluidic channels with an array of nanochannels by 2PP. Finally, the resulting SU-8 structure was used as a mold to produce nanofluidics out of polydimethylsiloxane (PDMS) by soft lithography, as shown in Fig. 30.8. Two microchannels were connected with three arrays of 16 nanochannels with a width of 420 nm and a length of 75 μm.

2PP has been used to integrate nanochannels in a closed glass microfluidic channel for cancer cell migration research [31]. Specifically, a T-shaped glass

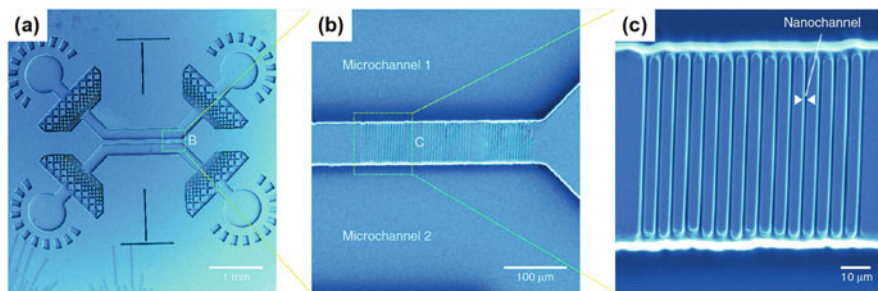


Fig. 30.8 Fabrication of nanofluidics by 2PP combined with conventional UV photolithography. (a) SEM micrograph of overview of fabricated nanofluidics. (b) SEM micrograph enlarged from the yellow rectangle in (a), showing three nanofluidic areas with 75- μm -long nanochannels joining the two microchannels. (c) SEM micrograph enlarged from the yellow rectangle in (b), showing 420-nm-wide nanochannels imprinted in PDMS [61]. (Reproduced with permission from Springer Nature. ©2019 by Springer Nature)

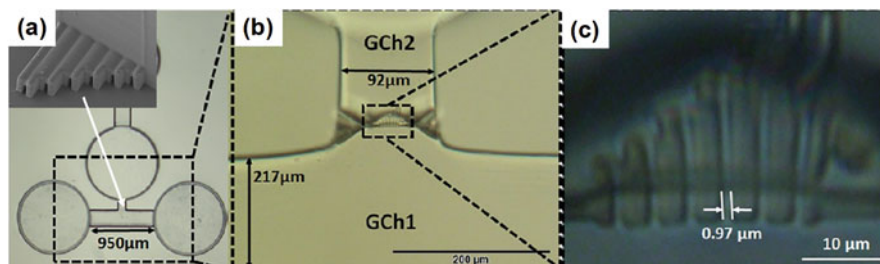


Fig. 30.9 Fabrication of nanofluidics by hybrid subtractive and additive femtosecond laser 3D processing (FLAE + 2PP). (a) Optical micrograph of the glass microfluidic platform fabricated by FLAE. Inset is an SEM micrograph of the polymer nanochannel array scaffold integrated at the junction of glass microfluidics by 2PP. (b) Optical micrograph enlarged from the dashed rectangle in (a). (c) Optical micrograph enlarged from the dashed rectangle in (c). The panpipe-shaped scaffold, consisting of six nanochannels with lengths of 6, 8, 11, 14, 18, and 21 μm , is integrated by 2PP at the junction of glass microchannels [31]. (Reproduced with permission from the American Chemical Society. ©2018 by ACS)

microfluidic platform (Fig. 30.9a) was fabricated inside photosensitive glass by FLAE. Then, SU-8 was introduced into the glass microfluidic structure to perform 2PP inside the closed microchannel. This two-step process has been termed hybrid subtractive and additive femtosecond laser 3D processing, which combines the best features of each process. However, the fabrication resolution of in-channel 2PP was significantly degraded owing to severe spherical aberration, because the laser beam propagated in three different refractive index media: index-matching oil for the objective lens, glass, and SU-8. To improve the fabrication resolution and thereby fabricate the nanochannels inside the glass microchannel, the wavefront of the laser beam was corrected by using a spatial light modulator so as to compensate for the spherical aberration. As a result, a panpipe-shaped polymer nanochannel array (inset

in Fig. 30.9a) was successfully integrated at the junction of the T-shaped glass microfluidic channels (Fig. 30.9b). The width of the integrated nanochannels was measured to be about 900 nm (Fig. 30.9c).

4 Applications of Nanofluidics Fabricated by Femtosecond Laser

The nanoscale fabrication resolution of femtosecond laser processing has yielded material topographies, morphologies, and structures suitable for the fabrication of functional nanofluidics. Nanofluidics fabricated by femtosecond lasers have been used in a variety of applications, such as fabricating fluid mixers in complex 3D microscale analysis systems [14], bacteria trapping [57], DNA stretching [15], and studying cancer cell migration [31, 60].

Liquid-assisted femtosecond laser drilling of fused silica was applied to a simple 3D fluid mixer [14]. Efficient mixing of fluids is crucial for micro- and nanofluidic systems, since a laminar flow is usually generated in the microchannel. For efficient mixing, the two different fluids were divided into four nanochannels (Fig. 30.10a, b). The 3D fabrication capability enables the crisscrossing architecture to interdigitate the two fluids at the outflow of the nanochannels. This architecture increased the area of the fluid-fluid interface to enhance the diffusion of each fluid for mixing. The nanoscale geometry of each fluid stream produced by the nanochannels further accelerated the mixing because the mixing time is proportional to the square of the diffusion distance (Fig. 30.10c).

Fused silica nanochannels with a minor axis of 200 nm fabricated by single-nanoplasma-assisted FLAE were used to trap bacteria [57]. *B. subtilis* was able to be trapped at the nanochannel inlets, since the minor axis of *B. subtilis* (500 nm) was significantly larger than that of the nanochannels.

Single-molecule behavior, specifically DNA stretching, was investigated by using nanochannels fabricated by liquid-assisted femtosecond laser drilling of porous glass based on the nanoplasma shown in Fig. 30.6 [15]. Figure 30.11a, b shows typical images of λ DNA stretched in the nanochannels owing to capillary force. In nanochannels whose cross-sections were elliptical (minor axis, 50 nm; major axis, 1.2 μm), the average stretching lengths of DNA molecules were measured to be about $6.4 \pm 1.0 \mu\text{m}$ (about 30% of dye-adjusted contour length) (Fig. 30.11a); the corresponding figure was about $2.8 \pm 0.6 \mu\text{m}$ (about 13% of dye-adjusted contour length) in nanochannels whose minor and major axes were 200 nm and 1.2 μm , respectively (Fig. 30.11b). Figure 30.11b also shows that some DNA molecules can be stretched to as long as about 15 μm , which is attributable to the clustering of DNA molecules. It was confirmed that the continuous flow ensured uniform stretching of the DNA molecules in the nanochannel arrays thanks to the continuity of the nanochannels and the repeatability of femtosecond laser processing. It is worth mentioning that control of DNA stretching in nanochannels

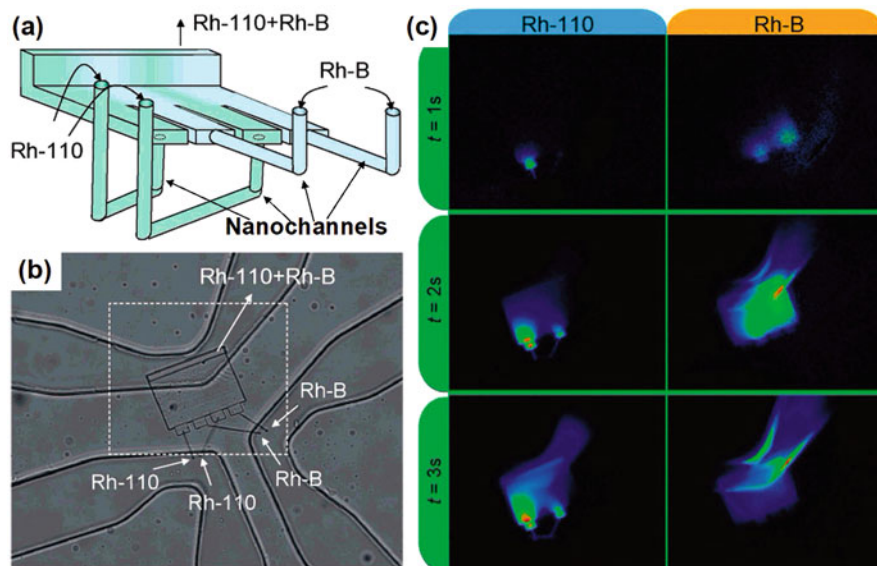


Fig. 30.10 Nanofluidic mixer fabricated by liquid-assisted femtosecond laser drilling of fused silica. (a) Schematic of nanofluidic mixer. (b) Optical micrograph of the fabricated nanofluidics. The three chevron-shaped channels are microfluidic channels (cast in PDMS, placed atop a glass coverslip) that serve as reservoirs. Fluids are drawn through nanochannels and mixed in the wide, flat, rectangular ($65 \times 52.5 \mu\text{m}$) cavity. Both the nanochannels and the cavity were fabricated by liquid-assisted femtosecond laser drilling. A 10-V potential is applied to the chip reservoirs, creating electroosmotic flows (arrows). (c) Time-lapse images taken after the potential is applied, showing mixing of fluorescent dyes Rhodamine-110 (Rh-110) and Rhodamine-B (Rh-B) [14]. (Reproduced with permission from the American Chemical Society. ©2005 by ACS)

has attracted much attention recently because of its potential application to analysis and manipulation of single molecules for DNA mapping and barcoding, for which the dimension of nanochannel narrower than the biomolecule persistence length ($\sim 50 \text{ nm}$) is essential.

Nanofluidics fabricated by hybrid subtractive and additive femtosecond laser 3D processing (Fig. 30.9) [31] and FLAE of photosensitive glass with post-thermal treatment for channel narrowing (Fig. 30.7) [60] were employed to elucidate the mechanism of human cancer cell migration during metastasis and invasion. In the early stages of metastasis formation and cancer cell invasion, cells must undergo large morphological changes in order to cross the basement membrane and then move through connective tissues to reach blood vessels or lymphatic vessels, since the typical size of cancer cells is several micrometers to several tens of micrometers, which is significantly larger than the space between connective tissues. However, it is still unknown how cancer cells can deform to migrate into narrower spaces, whether the cell nucleus can also be deformed during the migration and, if so, how the cells can survive the migration. Recent research has elucidated the migration behavior of cancer cells in narrow spaces [62, 63]. Femtosecond laser 3D processing

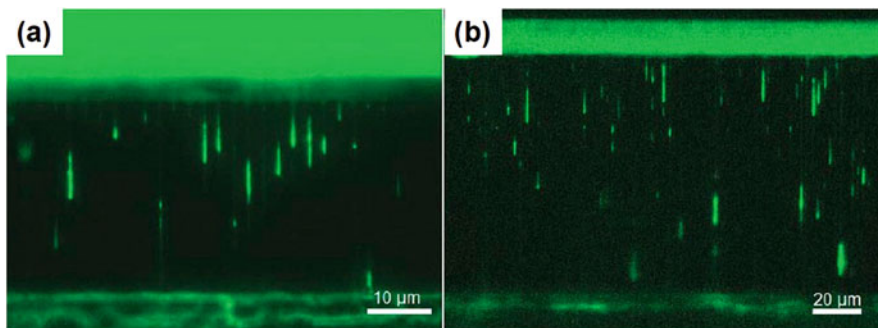


Fig. 30.11 Fluorescence images of λ DNA stretched in nanochannels with widths of (a) 50 nm and (b) 200 nm, fabricated by liquid-assisted femtosecond laser drilling of porous glass [15]. (Reproduced with permission from the Royal Society of Chemistry. ©2013 by RSC)

is a promising approach to creating platforms for cancer cell migration research, because it can construct true 3D configurations with nanometric dimensions, which could provide an unprecedented biomimetic environment for studying cancer cell migration. Such nanofluidics revealed the capability of human prostate cancer (PC3) cells to penetrate consecutive nanoscale constrictions *in vivo*. Extensive (approx. 50 μm) nucleus stretching was observed in cells migrating through nanochannels while keeping their viability (Fig. 30.12a, b). It was further observed that the cell body was compressed to a thin sheetlike shape to occupy the entire nanochannel from the entrance to the exit, while the cell nucleus deformed to a disklike shape was pulled into the nanochannel later and migrated. Cancer migration research using nanofluidics revealed many new findings, which include the following:

1. Cells can migrate in nanochannels with a width narrower than 1 μm , which is more than one order of magnitude narrower than the cell size.
2. Cells can migrate in nanochannels even without chemoattractant.
3. Cells are 100% viable and active after migration in nanochannels.
4. Cells can attain speeds of up to 1.5 $\mu\text{m}/\text{min}$, and their speed depends on the channel width: the narrower, the faster.
5. The volume of the cell nucleus is compressed, as it passes through nanochannels, and the cell nuclei can stretch over the length of a 50- μm -long nanochannel with no damage.
6. The cells can divide and proliferate after, and even during, migration. The probability of proliferation remains unchanged after migration.
7. The cells can migrate again through another nanochannel after the first migration, mimicking intravasation and extravasation.

Although ability of cancer cells to migrate in nanochannels narrower than 1 μm has been confirmed, it's very interesting to explore how narrow the channel the cells can migrate. Meanwhile, hybrid femtosecond laser 3D processing can create much more complicated structures to mimic micro- and nanostructures inside the human

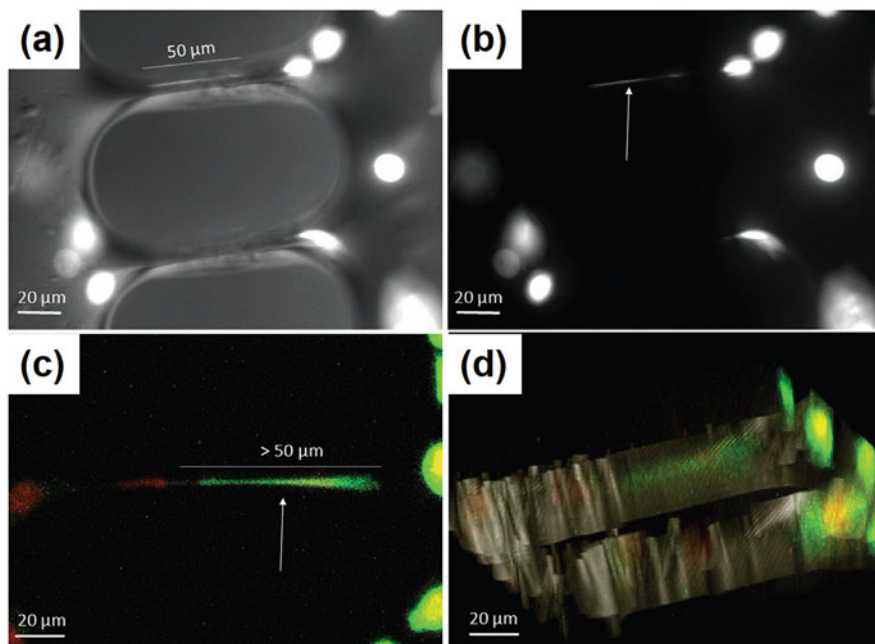


Fig. 30.12 Observation of cancer cells migrating in nanochannels fabricated by FLAE with post-thermal treatment. **(a, b)** Grayscale fluorescence micrographs of cell nuclei stained with red fluorescent protein, showing invasion into the narrow regions of the nanochannels. Fluorescence image is merged with optical micrograph in **(a)**. The white arrow in **(b)** shows an elongated cell nucleus inside the nanochannel. **(c)** 2D and **(d)** 3D confocal fluorescence micrographs of cells additionally stained with green fluorescent protein as a membrane marker, showing cancer cells migrating in the nanochannels by elongating both their nuclei and entire bodies with no damage to nuclear envelopes or cell membranes [60]. (Reproduced with permission from Wiley. ©2020 by Wiley)

body. Furthermore, 2PP integration of 3D protein structures instead of polymer could provide more biomimetic environment for this study. Further investigation using such functional nanofluidics is expected to be of great help in elucidating the metastasis mechanism of cancer cells.

5 Summary and Outlook

Nowadays, microfluidic systems are widely used for medical, biological, and chemical studies. Downsizing the dimensions to the nanoscale is increasingly demanded to provide a new generation of analytical tools in these fields. Nanofluidic systems with such small spaces offer ultrasensitive analysis at the single-cell and single-molecule level. In fact, they enable label-free identification and characterization of

single-stranded genomic DNA or RNA with no amplification procedure, as well as DNA sequencing. Additionally, mass transport in such small spaces can lead to new phenomena, such as enhanced mass flow rate and highly selective molecular transport.

Since critical issues of nanofluidic systems consist of fouling and clogging, future studies may concentrate on design and fabrication of smart geometries for efficient cell/molecule separations and DNA sequencing. Integration of nanofluidic systems with microchannels will become compulsory for many applications. Femtosecond lasers are a promising technology to fulfill those requirements for the fabrication of nanofluidic systems owing to their 3D fabrication capability with a wide range of manufacturable size from several tens of nanometers to several millimeters. Different kinds of femtosecond laser 3D processes, including liquid-assisted femtosecond laser drilling, FLAE, and 2PP, are available for nanofluidic fabrication. Although the fabrication resolution of femtosecond laser processing is inferior to other techniques, such as lithography using electron or ion beam and soft lithography, the fabrication capability of complex 3D structures provides a distinct advantage in creating unique structures and mimicking biological environments. The typical fabrication resolution of femtosecond laser processing is 100 nm for 2PP and several hundred nanometers for ablation. Particular efforts have been made to create nanochannels with widths narrower than 50 nm, for which a single nanoplasma was generated by precise control of the pulse energy in nanoripple formation. Nanofluidics fabricated by femtosecond laser processing has been applied to fluid mixers, bacteria trapping, DNA stretching, and the study of cancer cell migration. One expected application of nanofluidics is single-cell genomic analysis for personalized cancer therapies. Biopsies from cancer tumors harvested from patients will be analyzed using nanofluidic systems. The evaluation of cell population behavior could be correlated with the degree of migration and invasiveness and genomic analysis at a single-cell level. Specific doses of radiation therapy, chemotherapy, immunotherapy, and combinations thereof can then be examined.

The versatility of femtosecond laser processing may enable the fabrication of new nanofluidic systems composed of graded or hierarchical configurations with different dimensions from hundreds of micrometers down to a few tens of nanometers. These systems can be further integrated with functional micro- and nanocomponents such as optics and fluid control components by using different types of femtosecond laser processing. Hybrid approaches will be highly attractive for the fabrication of such functional nanofluidic systems, which will open new avenues for nanofluidic applications for single-cell and single-molecule analysis, drug screening, and the discovery or testing of personalized therapies using patient-derived cells. Further improvement of the fabrication resolution down to a couple of tens of nanometers will diversify nanofluidic applications of femtosecond laser processing.

References

1. E.K. Sackmann, A.L. Fulton, D.J. Beebe, *Nature* **507**, 181–189 (2014)
2. J.C.T. Eijkel, A. Berg, *Microfluid Nanofluidics* **1**, 249–267 (2005)
3. F. Sima, K. Sugioka, *Nanophotonics* **10**, 2389–2406 (2021)
4. J.H. Burnett, S.G. Kaplan, E.L. Shirley, P.J. Tompkins, J.E. Webb, *Proc. SPIE* **5754**, 611–621 (2005)
5. A.J. Storm, J.H. Chen, X.S. Ling, H.W. Zandbergen, C. Dekker, *Nat. Mater.* **2**, 537–540 (2003)
6. J. Li, S. Derek, M. Ciaran, B. Daniel, J.A. Michael, A.G. Jene, *Nature* **412**, 166–169 (2001)
7. D. Qin, X. Younan, M.W. George, *Nat. Protoc.* **5**, 491–502 (2010)
8. K. Sugioka, Y. Cheng, *MRS Bull.* **36**, 1020–1027 (2011)
9. K. Sugioka, Y. Cheng, *Lab Chip* **12**, 3576–3589 (2012)
10. K. Sugioka, J. Xu, D. Wu, Y. Hanada, Z. Wang, Y. Cheng, K. Midorikawa, *Lab Chip* **14**, 3447–3458 (2014)
11. F. Sima, J. Xu, D. Wu, K. Sugioka, *Micromachines* **8**, 40 (2017)
12. F. Sima, K. Sugioka, R. Martínez Vázquez, R. Osellame, L. Kelemen, P. Ormos, *Nanophotonics* **7**, 613–634 (2018)
13. R. Osellame, H.J. Hoekstra, G. Cerullo, M. Pollnau, *Laser Photonics Rev.* **5**, 442–463 (2011)
14. K. Ke, E.F. Hasselbrink, A.J. Hunt, *Anal. Chem.* **77**, 5083–5088 (2005)
15. Y. Liao, Y. Cheng, C. Liu, J. Song, F. Hei, Y. Shen, D. Chen, Z. Xu, Z. Fan, X. Wei, K. Sugioka, K. Midorikawa, *Lab Chip* **13**, 1626–1631 (2013)
16. Y. Li, K. Itoh, W. Watanabe, K. Yamada, D. Kuroda, J. Nishii, Y. Jiang, *Opt. Lett.* **26**, 1912–1914 (2001)
17. Y. Li, S. Qu, *Curr. Appl. Phys.* **13**, 1292–1295 (2013)
18. A. Marcinkevičius, S. Juodkazis, M. Watanabe, M. Miwa, S. Matsuo, H. Misawa, J. Nishii, *Opt. Lett.* **26**, 277–279 (2001)
19. M. Masuda, K. Sugioka, Y. Cheng, N. Aoki, M. Kawachi, K. Shihoyama, K. Toyoda, H. Helvajian, K. Midorikawa, *Appl. Phys.* **A76**, 857–860 (2003)
20. Y. Bellouard, A. Said, M. Dugan, P. Bado, *Opt. Express* **12**, 2120–2129 (2004)
21. K.C. Vishnubhatla, N. Bellini, R. Ramponi, G. Cerullo, R. Osellame, *Opt. Express* **17**, 8685–8695 (2009)
22. S. Maruo, O. Nakamura, S. Kawata, *Opt. Lett.* **22**, 132–134 (1997)
23. S. Kawata, H.B. Sun, T. Tanaka, K. Takada, *Nature* **412**, 697–698 (2001)
24. K.K. Seet, V. Mizeikis, S. Matsuo, S. Juodkazis, H. Misawa, *Adv. Mater.* **17**, 541–545 (2005)
25. S. Maruo, J.T. Fourkas, *Laser Photonics Rev.* **2**, 100–111 (2008)
26. D. Wu, S. Wu, J. Xu, L. Niu, K. Midorikawa, K. Sugioka, *Laser Photonics Rev.* **8**, 458–467 (2014)
27. D. Wu, J. Xu, L. Niu, S. Wu, K. Midorikawa, K. Sugioka, *Light Sci. Appl.* **4**, e228 (2015)
28. L. Jonušauskas, S. Rekštyte, R. Buividas, S. Butkus, R. Gadonas, S. Juodkazis, M. Malinauskas, *Opt. Eng.* **56**, 094108 (2017)
29. T. Tičkūnas, M. Perrenoud, S. Butkus, R. Gadonas, S. Rekštytė, M. Malinauskas, D. Paipulas, Y. Bellouard, V. Sirutkaitis, *Opt. Express* **25**, 26280–26288 (2017)
30. K. Sugioka, *Int. J. Extreme Manuf.* **1**, 012003 (2019)
31. F. Sima, H. Kawano, A. Miyawaki, L. Kelemen, P. Ormos, D. Wu, J. Xu, K. Midorikawa, K. Sugioka, *ACS Appl. Bio Mater.* **1**, 1667–1676 (2018)
32. W.S. Fan, R. Storz, H.W. Tom, J. Bokor, *Phys. Rev.* **B46**, 13592–13595 (1992)
33. S.S. Wellershoff, J. Hohlfeld, J. Gädde, E. Matthias, *Appl. Phys.* **A69**, S99–S107 (1999)
34. K. Sugioka, Y. Cheng, *Light Sci. Appl.* **3**, e149 (2014)
35. N. Bloembergen, *J. Nonlinear Opt. Phys.* **6**, 377–385 (1997)
36. B.C. Stuart, M.D. Feit, A.M. Rubenchik, B.W. Shore, M.D. Perry, *Phys. Rev. Lett.* **74**, 2248–2251 (1995)
37. A.P. Joglekar, H. Liu, E. Meyhöfer, G. Mourou, A.J. Hunt, *Proc. Natl. Acad. Sci.* **101**, 5856–5861 (2004)

38. K. Sugioka, Y. Cheng, *Appl. Phys. Rev.* **1**, 041303 (2014)
39. S. Nakashima, K. Sugioka, K. Midorikawa, *Appl. Phys.* **A101**, 475–481 (2010)
40. K.M. Davis, K. Miura, N. Sugimoto, K. Hirao, *Opt. Lett.* **21**, 1729–1731 (1996)
41. E.N. Glezer, M. Milosavljevic, L. Huang, R.J. Finlay, T.-H. Her, J.P. Callan, E. Mazur, *Opt. Lett.* **21**, 2023–2025 (1996)
42. W. Watanabe, T. Asano, K. Yamada, K. Itoh, J. Nishii, *Opt. Lett.* **28**, 2491–2493 (2003)
43. J. Zhang, M. Gecevičius, M. Beresna, P.G. Kazansky, *Phys. Rev. Lett.* **112**, 033901 (2014)
44. A. Ishikawa, T. Tanaka, S. Kawata, *Appl. Phys. Lett.* **89**, 113102 (2006)
45. S. Maruo, T. Saeki, *Opt. Express* **16**, 1174–1179 (2008)
46. D. Serien, K. Sugioka, *Opto-Electron. Adv.* **1**, 180008 (2018)
47. D. Serien, K. Sugioka, *ACS Biomater. Sci. Eng.* **6**, 1279–1287 (2020)
48. W.H. Zhou, S.M. Kuebler, K. Braun, T.Y. Yu, J.K. Cammack, C.K. Ober, J.W. Perry, S.R. Marder, *Science* **296**, 1106 (2002)
49. Y. Liao, Y. Ju, L. Zhang, F. He, Q. Zhang, Y. Shen, D. Chen, Y. Cheng, Z. Xu, K. Sugioka, K. Midorikawa, *Opt. Lett.* **35**, 3225 (2010)
50. F. Costache, M. Henyk, J. Reif, *Appl. Surf. Sci.* 208–209, 486–491 (2003)
51. Y. Shimotsuma, P.G. Kazansky, J. Qiu, K. Hirao, *Phys. Rev. Lett.* **91**, 247405 (2003)
52. V.R. Bhardwaj, E. Simova, P.P. Rajeev, C. Hnatovsky, R.S. Taylor, D.M. Rayner, P.B. Corkum, *Phys. Rev. Lett.* **96**, 057404 (2006)
53. K. Sugioka, *Nanophotonics* **5**, 17–37 (2016)
54. M. Hörstmann-Jungemann, J. Gottmann, M. Keggenhoff, *J. Laser Micro Nanoeng.* **5**, 145–149 (2010)
55. D. Choudhury, A. Rodenas, L. Paterson, F. Díaz, D. Jaque, A.K. Kar, *Appl. Phys. Lett.* **103**, 041101 (2013)
56. O. Tokel, A. Turnali, G. Makey, P. Elahi, T. Çolakoğlu, E. Ergeçen, Ö. Yavuz, R. Hübner, M.Z. Borra, I. Pavlov, A. Bek, R. Turan, D.K. Kesim, S. Tozburun, S. İlday, F.Ö. İlday, *Nat. Photonics* **11**, 639–645 (2017)
57. O. Nukaga, S. Yamamoto, K. Tabata, T. Kubota, S. Samukawa, M. Sugiyama, *Proc. 14th μ TAS* 1199–1201 (2010)
58. S. Kiyama, S. Matsuo, S. Hashimoto, Y. Morihira, *J. Phys. Chem.* **C113**, 11560 (2009)
59. Y. Cheng, K. Sugioka, K. Midorikawa, M. Masuda, K. Toyoda, M. Kawachi, K. Shihoyama, *Opt. Lett.* **28**, 1144–1146 (2003)
60. F. Sima, H. Kawano, M. Hirano, A. Miyawaki, K. Obata, D. Serien, K. Sugioka, *Adv. Mater. Technol.* **5**, 2000484 (2020)
61. O. Vanderpoorten, Q. Peter, P.K. Challa, U.F. Keyser, J. Baumberg, C.F. Kaminski, T.P.J. Knowles, *Microsyst. Nanoeng.* **5**, 40 (2019)
62. C.M. Denais, R.M. Gilbert, P. Isermann, A.L. McGregor, M. Lindert, B. Weigelin, P.M. Davidson, P. Friedl, K. Wolf, J. Lammerding, *Science* **352**, 353–358 (2016)
63. D. Truong, J. Puleo, A. Llave, G. Mounemne, R.D. Kamm, M. Nikkhah, *Sci. Rep.* **6**, 34094 (2016)